

Short Communication

## Magnetic Properties, Microstructure and Corrosion Resistance of Ce-doped $\text{Sm}_{1-x}\text{Ce}_x(\text{Co}_{\text{bal}}\text{Fe}_{0.14}\text{Cu}_{0.07}\text{Zr}_{0.05})_{7.5}$ Magnets

Changquan Zhou<sup>1</sup>, Yong Gu<sup>2,\*</sup>, Minxiang Pan<sup>3</sup>

<sup>1</sup> Zhejiang University of Water Resources and Electric Power, Hangzhou 310018, P. R. China

<sup>2</sup> Qianjiang College, Hangzhou Normal University, Hangzhou 310036, P. R. China

<sup>3</sup> China Jiliang University, Hangzhou 310018, P. R. China

\*E-mail: [guyonghz@126.com](mailto:guyonghz@126.com)

Received: 21 October 2019 / Accepted: 28 November 2019 / Published: 31 December 2019

The influence of the Ce content and the relation among the magnetic properties, corrosion resistance and microstructure of the  $\text{Sm}_{1-x}\text{Ce}_x(\text{Co}_{\text{bal}}\text{Fe}_{0.14}\text{Cu}_{0.07}\text{Zr}_{0.05})_{7.5}$  magnets are systemically studied. The enhanced magnetic properties ( $B_r = 11.01$  kG,  $H_{cj} = 15.5$  kOe, and  $(BH)_{\text{max}} = 30.1$  MGOe) have been obtained with the slight Ce-doped ( $x = 0.1$ ). The lower values of the corrosion potential  $E_{\text{corr}}$  and corrosion current density  $i_{\text{corr}}$  for the Ce-doped magnet indicate that electrochemical corrosion rate of the Ce-doped magnet slows down and the corrosion resistance of the magnet is stronger. The microstructure results show that the Ce-doped magnet obtains a more uniform cellular structure with the smaller cell size and the homogeneous cell boundary phase, while the content of the Ce shows no observable difference between the cell and cell boundary.

**Keywords:** Corrosion; SmCo; Ce; Magnetic properties; Cell size

### 1. INTRODUCTION

With the continuous improvement of productivity, people have higher requirements for the application of permanent magnet materials [1]. In recent years, with the rapid development of aerospace technology, it requires that the use temperature of permanent magnet materials is more than 450 °C [2-4]. However, the Curie temperature of NdFeB permanent magnet is only about 300 °C, and the magnetic property decays rapidly with the increase of temperature, and its operating temperature is basically below 150 °C. Although AlNiCo permanent magnet material can meet this temperature requirement, while the magnetic properties are very low and cannot meet the use requirements. As the reason of the high Curie temperature, magnetocrystalline anisotropy and saturation magnetization, rare-earth cobalt based intermetallics ( $\text{SmCo}_5$  and  $\text{Sm}_2\text{Co}_{17}$ ) have been widely studied since they were discovered in the 1960s [5-10]. They can be used as sintered and bonded magnets with high temperature stability and high service

temperature. The successful examples in this regard are the commercialized 2:17-based  $\text{Sm}(\text{Co}, \text{Fe}, \text{Cu}, \text{Zr})_Z$  magnets.

In 1980s, many researchers studied the  $\text{Sm}_2\text{Co}_{17}$  sintered permanent magnet doped with heavy rare earth elements, such as Gd, Ho, Er, Tb and Dy, although the overall magnetic properties of the  $\text{Sm}_2\text{Co}_{17}$  magnets are relatively low [11-15]. Meanwhile, the temperature coefficient of  $\text{Sm}_2\text{Co}_{17}$  sintered permanent magnet prepared by replacing Sm with Er is very low. The magnetic properties are as follows: remanence  $B_r = 9.4$  kG,  $H_{cj} = 413.9$  kA/m, and the magnetic energy product  $(BH)_{\max} = 18$  MGOe. The research on the preparation of  $\text{Sm}_2\text{Co}_{17}$  sintered permanent magnet by doping heavy rare earth elements mainly focuses on the preparation of  $\text{Sm}_2\text{Co}_{17}$  sintered permanent magnet with low temperature coefficient. There are few reports on the preparation of high performance  $\text{Sm}_2\text{Co}_{17}$  sintered permanent magnet by doping light rare earth elements. The results show that the intrinsic magnetic properties of CeCo are similar to those of SmCo, and more importantly, the reserves of Ce are abundant and the price is much cheaper than that of Sm [19-20]. Therefore, it is of great significance to replace Sm with Ce in the preparation of SmCo based permanent magnetic materials.

In order to further enhance the magnetic properties of the  $\text{Sm}(\text{Co}_{\text{bal}}\text{Fe}_{0.14}\text{Cu}_{0.07}\text{Zr}_{0.05})_{7.5}$  magnets, the  $\text{Sm}_{1-x}\text{Ce}_x(\text{Co}_{\text{bal}}\text{Fe}_{0.14}\text{Cu}_{0.07}\text{Zr}_{0.05})_{7.5}$  with  $x = 0, 0.1$  and  $0.2$  were fabricated by a traditional powder metallurgical technology and systemically investigated. Meanwhile, the relation among the magnetic properties, corrosion resistance and microstructure of the  $\text{Sm}_{1-x}\text{Ce}_x(\text{Co}_{\text{bal}}\text{Fe}_{0.14}\text{Cu}_{0.07}\text{Zr}_{0.05})_{7.5}$  magnets were studied. This will lay a solid theoretical and experimental foundation for optimizing and improving the high temperature service characteristics of SmCo permanent magnet materials, reducing the cost of magnets and developing a new generation of permanent magnet materials with higher service temperature.

## 2. EXPERIMENTAL PART

The samples with the nominal compositions of  $\text{Sm}_{1-x}\text{Ce}_x(\text{Co}_{\text{bal}}\text{Fe}_{0.14}\text{Cu}_{0.07}\text{Zr}_{0.05})_{7.5}$  ( $x = 0, 0.1$  and  $0.2$ ) with different Ce content were fabricated by a traditional powder metallurgical technology. The particle size was about  $70 \mu\text{m}$  after coarse and medium crushing, and then the ball milling with high purity gasoline as the medium was used for 12 hours. The powders were oriented and shaped by magnetic field forming press with the magnetic field up to 2 T and the pressure is 300 MPa after cold isostatic pressure. The green compactions were sintered at  $1210\sim 1250$  °C for 2 h and then homogenized at 1180 °C for 2h. The isothermal aging temperature was 820 °C for 6 h and cooling to 380 °C for 6 h with the cooling rate is  $1$  °C / min, then quenched to the room temperature by the water.

The phase structures of the magnets were carried out by the Rigaku D/max 2500 X-ray diffraction (XRD) with a Cu  $K\alpha$  radiation (The wavelength of X-ray is  $\lambda = 1.5406$  Å, the scanning angle range is  $20^\circ \sim 80^\circ$ , the scanning step length is  $0.02^\circ$ , and the scanning speed is  $1^\circ/\text{min}$ ). The magnetic properties of the SmCo magnets ( $\Phi 10 \times 10$  mm) were accomplished by the Pulsed Field Magnetometer (PFM) with a maximum applied field of 7.5 T. The microstructure of the final magnets was analyzed by FEI Technai F20 Transmission Electron Microscope (TEM). The polarization curves were measured by the

electrochemical workstation (PARSTAT 2273) under 2.5 wt.% NaCl aqueous solution with a scan rate of 1 mV/s.

### 3. RESULTS AND DISCUSSION

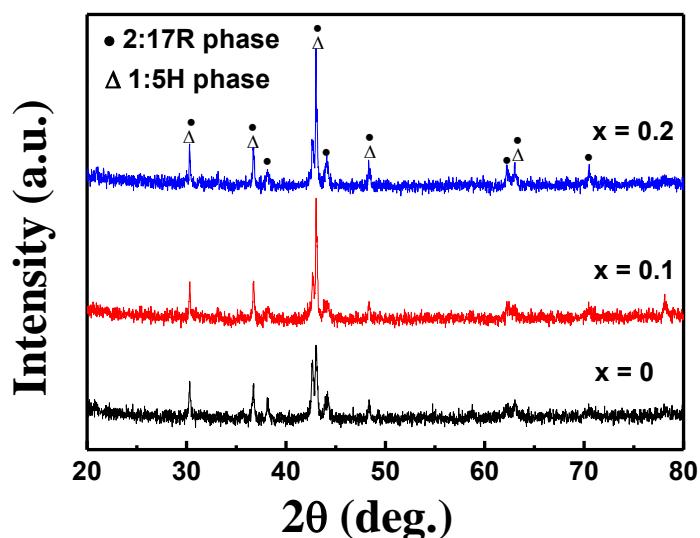


**Figure 1.** XRD patterns of the  $\text{Sm}_{1-x}\text{Ce}_x(\text{Co}_{\text{bal}}\text{Fe}_{0.14}\text{Cu}_{0.07}\text{Zr}_{0.05})_{7.5}$  ( $x = 0, 0.1$  and  $0.2$ ) magnets.

Figure 1 presents the XRD patterns of the  $\text{Sm}_{1-x}\text{Ce}_x(\text{Co}_{\text{bal}}\text{Fe}_{0.14}\text{Cu}_{0.07}\text{Zr}_{0.05})_{7.5}$  ( $x = 0, 0.1$  and  $0.2$ ) magnets. According to the XRD results, it can be seen that the magnets of the Ce-free and Ce-doped magnets consist of two magnetic phases: the hexagonal 1:5H and the rhombohedral 2:17R magnetic phase. No observable difference was detected in the XRD patterns by Ce substituted. Similar behaviors were also observed in the heavy rare-earth (HRE) Lu substituted Sm-Co-Fe-Cu-Zr magnet [21].

Figure 2 shows the demagnetisation curves for the  $\text{Sm}_{1-x}\text{Ce}_x(\text{Co}_{\text{bal}}\text{Fe}_{0.14}\text{Cu}_{0.07}\text{Zr}_{0.05})_{7.5}$  ( $x = 0, 0.1$  and  $0.2$ ) magnets at room temperature. It can be seen that the Ce content has a great influence on the remanence ( $B_r$ ) and intrinsic coercivity ( $H_{cj}$ ). Meanwhile, the demagnetisation curves for the all magnets obtain a good hard-magnetic phase behavior, demonstrating that a good intergrain exchange-coupling in these samples and all the hard magnetic phases are uniformly reversed under the applied field. Table 1 gives the magnetic properties (remanence  $B_r$ , intrinsic coercivity  $H_{cj}$ , and maximum energy product  $(BH)_{\text{max}}$ ) of  $\text{Sm}_{1-x}\text{Ce}_x(\text{Co}_{\text{bal}}\text{Fe}_{0.14}\text{Cu}_{0.07}\text{Zr}_{0.05})_{7.5}$  ( $x = 0, 0.1$  and  $0.2$ ) magnets. As shown in Table 1, the corresponding magnetic properties of the Ce-free ( $x = 0$ )  $\text{Sm}_{1-x}\text{Ce}_x(\text{Co}_{\text{bal}}\text{Fe}_{0.14}\text{Cu}_{0.07}\text{Zr}_{0.05})_{7.5}$  is: the remanence  $B_r = 10.92$  kG, intrinsic coercivity  $H_{cj} = 13.8$  kOe, and maximum energy product  $(BH)_{\text{max}} = 28.6$  MGOe, while the magnetic properties has been enhanced ( $B_r = 11.01$  kG,  $H_{cj} = 15.5$  kOe, and  $(BH)_{\text{max}} = 30.1$  MGOe) with the slight Ce-doped ( $x = 0.1$ ). Furthermore, with the further increase of the Ce content, the magnetic properties ( $B_r = 10.95$  kG,  $H_{cj} = 12.6$  kOe, and  $(BH)_{\text{max}} = 29.4$  MGOe) of the SmCo magnet show a little decrease, while the magnetic properties are still higher than the Ce-free magnet. It suggests that the addition of Ce element can enhance the magnetic properties of the  $\text{Sm}_{1-x}\text{Ce}_x(\text{Co}_{\text{bal}}\text{Fe}_{0.14}\text{Cu}_{0.07}\text{Zr}_{0.05})_{7.5}$  magnet.

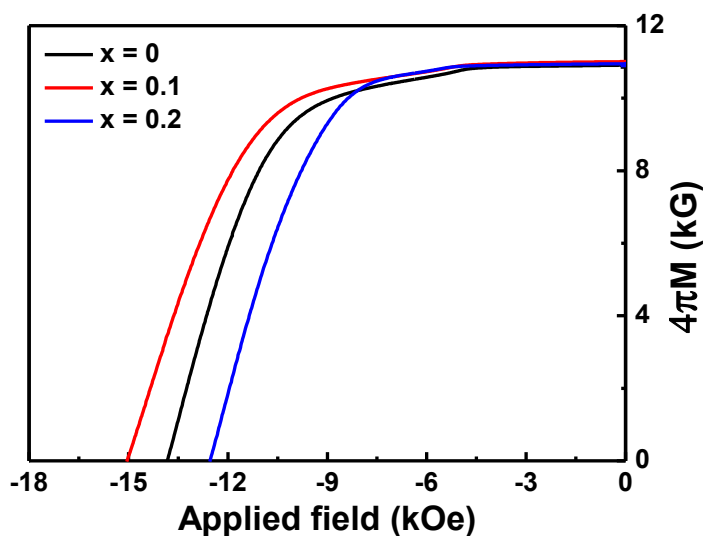


**Figure 2.** Demagnetisation curves for the  $\text{Sm}_{1-x}\text{Ce}_x(\text{Co}_{\text{bal}}\text{Fe}_{0.14}\text{Cu}_{0.07}\text{Zr}_{0.05})_{7.5}$  ( $x = 0, 0.1$  and  $0.2$ ) magnets at room temperature.

**Table 1.** Magnetic properties (remanence  $B_r$ , intrinsic coercivity  $H_{cj}$ , and maximum energy product  $(BH)_{\text{max}}$ ) of  $\text{Sm}_{1-x}\text{Ce}_x(\text{Co}_{\text{bal}}\text{Fe}_{0.14}\text{Cu}_{0.07}\text{Zr}_{0.05})_{7.5}$  ( $x = 0, 0.1$  and  $0.2$ ) magnets.

Alloys	$B_r$ (kG)	$H_{cj}$ (kOe)	$(BH)_{\text{max}}$ (MGOe)
$x = 0$	10.92	13.8	28.6
$x = 0.1$	11.01	15.5	30.1
$x = 0.2$	10.95	12.6	29.4

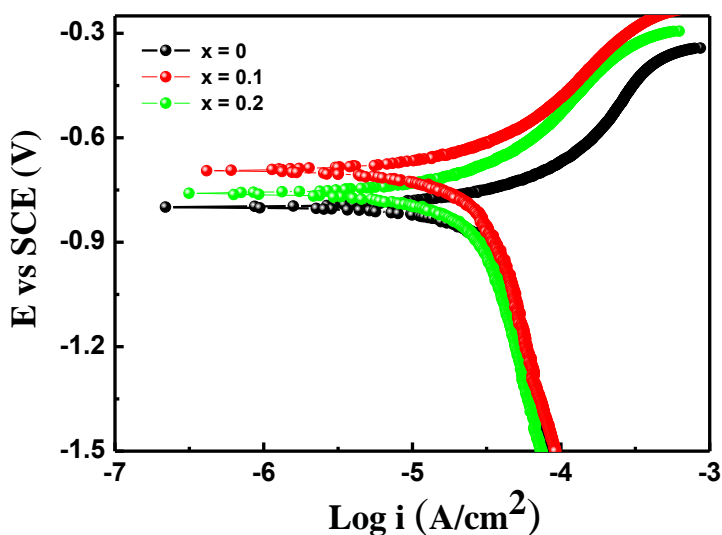


**Figure 3.** Potentiodynamic polarization curves in 2.5 wt.% NaCl aqueous solutions for the  $\text{Sm}_{1-x}\text{Ce}_x(\text{Co}_{\text{bal}}\text{Fe}_{0.14}\text{Cu}_{0.07}\text{Zr}_{0.05})_{7.5}$  ( $x = 0, 0.1$  and  $0.2$ ) magnets.

Figure 3 shows the potentiodynamic polarization curves in 2.5 wt.% NaCl aqueous solutions for the  $\text{Sm}_{1-x}\text{Ce}_x(\text{Co}_{\text{bal}}\text{Fe}_{0.14}\text{Cu}_{0.07}\text{Zr}_{0.05})_{7.5}$  ( $x = 0, 0.1$  and  $0.2$ ) magnets. The results show that the Ce-free ( $x = 0$ ) and the Ce-doped ( $x = 0.1, x = 0.2$ ) magnets exhibit typical hydrogen evolution polarization in the cathode region [22]. Meanwhile, the corrosion potential  $E_{\text{corr}}$  and corrosion current density  $i_{\text{corr}}$  for the  $\text{Sm}_{1-x}\text{Ce}_x(\text{Co}_{\text{bal}}\text{Fe}_{0.14}\text{Cu}_{0.07}\text{Zr}_{0.05})_{7.5}$  ( $x = 0, 0.1$  and  $0.2$ ) magnets are calculated by the Tafel extrapolation method [23, 24] and showed in Table 1. It can be seen that the corrosion potential  $E_{\text{corr}}$  of the Ce-doped ( $x = 0.1$ ) magnet is the highest, its corrosion potential  $E_{\text{corr}} = -0.681$  V, while the Ce-free ( $x = 0$ ) and the higher Ce-doped content magnet are lower, their corrosion potential are  $E_{\text{corr}} = -0.802$  V and  $E_{\text{corr}} = -0.768$  V, respectively. Furthermore, compared the Ce-free magnet, the corrosion current density  $i_{\text{corr}}$  of the Ce-doped ( $x = 0.1$ ) magnet is also decreased from  $31.23 \mu\text{A}/\text{cm}^2$  to  $17.24 \mu\text{A}/\text{cm}^2$ . The lower values of the corrosion potential  $E_{\text{corr}}$  and corrosion current density  $i_{\text{corr}}$  for the Ce-doped magnet indicate that electrochemical corrosion rate of the Ce-doped magnet slows down and the corrosion resistance of the magnet is stronger.

**Table 2.** The corrosion potential  $E_{\text{corr}}$  and corrosion current density  $i_{\text{corr}}$  for the  $\text{Sm}_{1-x}\text{Ce}_x(\text{Co}_{\text{bal}}\text{Fe}_{0.14}\text{Cu}_{0.07}\text{Zr}_{0.05})_{7.5}$  ( $x = 0, 0.1$  and  $0.2$ ) magnets.

Alloys	$E_{\text{corr}}(\text{V})$	$i_{\text{corr}}(\mu\text{A}/\text{cm}^2)$
$x = 0$	-0.802	31.23
$x = 0.1$	-0.681	17.24
$x = 0.2$	-0.768	20.02

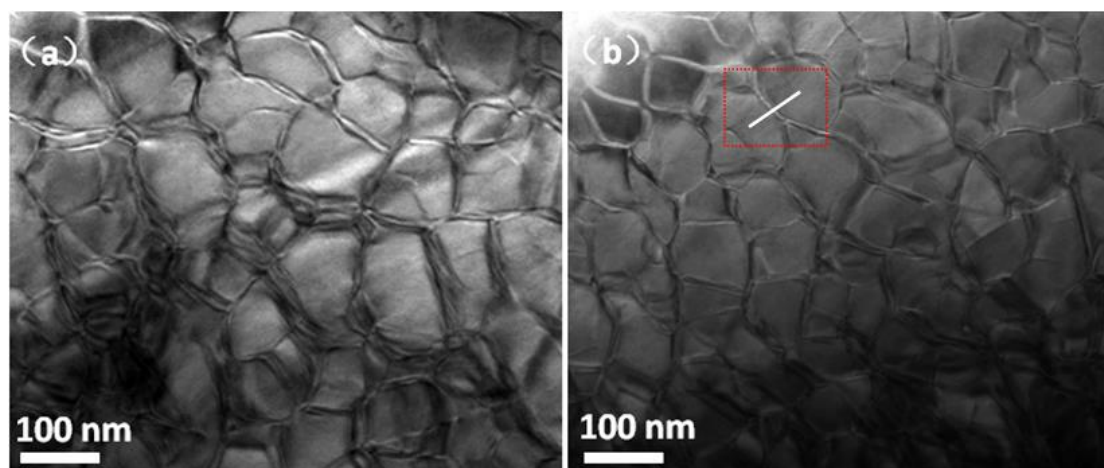


**Figure 4.** TEM images of the  $\text{Sm}_{1-x}\text{Ce}_x(\text{Co}_{\text{bal}}\text{Fe}_{0.14}\text{Cu}_{0.07}\text{Zr}_{0.05})_{7.5}$  ( $x = 0$  and  $0.1$ ) magnets along the  $[001]_{2:17R}$  zone axis.

The above results show that the Ce-doped magnet obtains the enhanced magnetic properties and the improved of the corrosion resistance. In order to investigate the relation among the magnetic properties, corrosion resistance and microstructure of the  $\text{Sm}_{1-x}\text{Ce}_x(\text{Co}_{\text{bal}}\text{Fe}_{0.14}\text{Cu}_{0.07}\text{Zr}_{0.05})_{7.5}$  magnets,

we selected magnets with Ce content at  $x = 0$  and  $0.1$  for detailed microstructural analysis. Figure 4 presents the TEM images of the  $\text{Sm}_{1-x}\text{Ce}_x(\text{Co}_{\text{bal}}\text{Fe}_{0.14}\text{Cu}_{0.07}\text{Zr}_{0.05})_{7.5}$  ( $x = 0$  and  $0.1$ ) magnets along the  $[001]_{2:17\text{R}}$  zone axis. It can be seen that the Ce-free and Ce-doped magnets have relatively complete cellular structure, and there is very thin cell wall structure around the cellular structure with a wall thickness of  $5 \sim 10$  nm. According to the Hadjipanayis results [25] that the cell size of the cellular structure is directly related to the magnetic properties of the magnet, and the large cell size and thick cell wall size are beneficial to the enhanced magnetic properties of the magnet. Meanwhile, according to the TEM results, it can be seen that the Ce-doped magnet obtains a more uniform cellular structure with the smaller cell size and the homogeneous cell boundary phase, which may lead to the higher coercivity and higher maximum energy product for the Ce-doped ( $x = 0.1$ ) magnet.

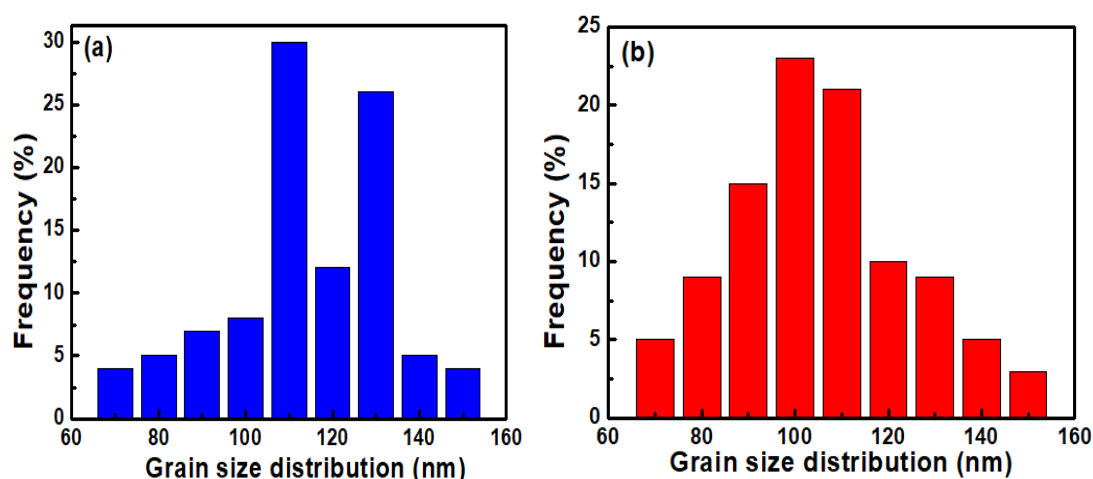


**Figure 5.** Distribution histograms of grain size for the  $\text{Sm}_{1-x}\text{Ce}_x(\text{Co}_{\text{bal}}\text{Fe}_{0.14}\text{Cu}_{0.07}\text{Zr}_{0.05})_{7.5}$  ( $x = 0$  and  $0.1$ ) magnets.

Additionally, the uniform cellular structure with the smaller cell size for the Ce-doped magnet can be seen more clearly from the distribution histograms of grain size corresponding to the TEM images. Figure 5 shows the distribution histograms of grain size for the  $\text{Sm}_{1-x}\text{Ce}_x(\text{Co}_{\text{bal}}\text{Fe}_{0.14}\text{Cu}_{0.07}\text{Zr}_{0.05})_{7.5}$  ( $x = 0$  and  $0.1$ ) magnets. Meanwhile, by comparing the distribution histograms of grain size for the Ce-free ( $x = 0$ ) and Ce-doped ( $x = 0.1$ ) magnets, it can be seen that the average cell size is  $115$  nm and  $100$  nm for the Ce-free and Ce-doped samples, respectively. It indicates that the Ce-doped magnet ( $x = 0.1$ ) obtains a smaller grain size and more homogeneous distribution of grain size.

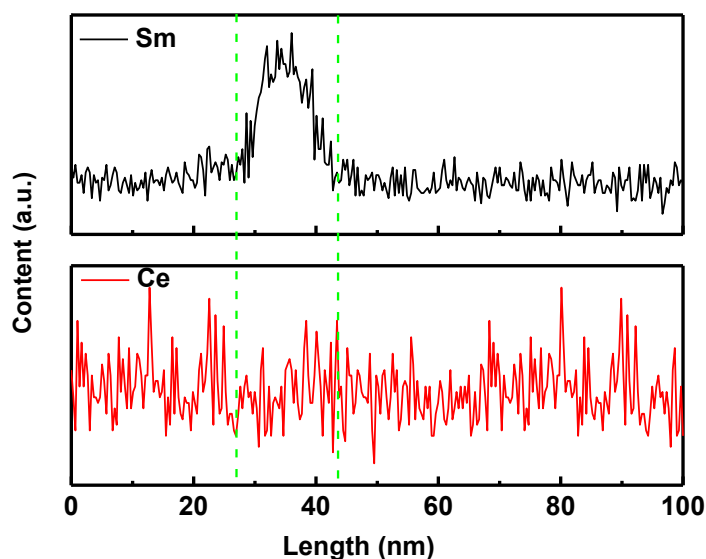


**Figure 6.** Line scan change tendency of the Sm and Ce element corrected line scanning in Fig. 4 (b).

The above results show that the Ce-doped magnet obtains the enhanced magnetic properties and the improved of the corrosion resistance. In order to further understand the mechanism of Ce-doped enhance the magnetic properties and the corrosion resistance, we have carried out the Sm and Ce element distribution across cell boundaries for Ce-doped magnet (as shown in Fig. 4 (b), the white line show the general range of cell wall). It can be seen from the Fig. 6 that the content of Sm is increased obviously in the cell wall when the line scan passed through the cell wall, while the content of the Ce shows no observable difference between the cell and cell boundary. It indicates that the homogeneously distribute of the Ce element in the cellular structure tends to result in the high performance of the magnetic properties.

The present results show that the  $\text{Sm}_{1-x}\text{Ce}_x(\text{Co}_{\text{bal}}\text{Fe}_{0.14}\text{Cu}_{0.07}\text{Zr}_{0.05})_{7.5}$  with proper Ce content can enhance the magnetic properties by due to the uniform cellular structure with the smaller cell size and the homogeneous cell boundary phase. In addition, the lower values of the corrosion potential  $E_{\text{corr}}$  and corrosion current density  $i_{\text{corr}}$  for the Ce-doped magnet indicate that electrochemical corrosion rate of the Ce-doped magnet slows down and the corrosion resistance of the magnet is stronger.

#### 4. CONCLUSION

The effect of Ce addition on the magnetic properties, corrosion resistance and microstructure of the  $\text{Sm}_{1-x}\text{Ce}_x(\text{Co}_{\text{bal}}\text{Fe}_{0.14}\text{Cu}_{0.07}\text{Zr}_{0.05})_{7.5}$  magnets are systemically studied. The enhanced magnetic properties ( $B_r = 11.01$  kG,  $H_{\text{cj}} = 15.5$  kOe, and  $(BH)_{\text{max}} = 30.1$  MGOe) have been obtained with the slight Ce-doped ( $x = 0.1$ ). Meanwhile, the  $\text{Sm}_{1-x}\text{Ce}_x(\text{Co}_{\text{bal}}\text{Fe}_{0.14}\text{Cu}_{0.07}\text{Zr}_{0.05})_{7.5}$  with proper Ce content can enhance the magnetic properties by due to the uniform cellular structure with the smaller cell size and the homogeneous cell boundary phase. In addition, the lower values of the corrosion potential  $E_{\text{corr}}$  and

corrosion current density  $i_{\text{corr}}$  for the Ce-doped magnet indicate that electrochemical corrosion rate of the Ce-doped magnet slows down and the corrosion resistance of the magnet is stronger.

#### ACKNOWLEDGEMENT

This work was supported by the Public Project of Zhejiang Province (LGC20E010004).

#### References

1. O. Gutfleisch, A.W. Matthew, E. Brück, C.H. Chen, S.G. Sankar, J.P. Liu, *Adv. Mater.*, 23 (2011) 821.
2. J.M.D. Coey, *IEEE Trans. Magn.*, 47 (2011) 4671.
3. J. Fidler, J. Bernardi, T. Schrefl, *Scr. Metal. Mater.*, 33 (1995) 1781.
4. X.H. Li, L. Lou, W.P. Song, G.W. Huang, F.C. Hou, Q. Zhang, H.T. Zhang, J.W. Xiao, B. Wen, X.Y. Zhang, *Adv. Mater.*, 29 (2017) 1606430.
5. E.A. Nesbit, *J. Appl. Phys.*, 30 (1959) 365.
6. W.M. Hubbard, E. Adams, J.V. Gilfrich, *J. Appl. Phys.*, 31 (1960) 368.
7. J.J. Becker, *IEEE Trans. Magn.*, 4 (1968) 239.
8. K.Strnat, G. Hoffer, J. Olson, W. Osterag, J.J. Becker, *J. Appl. Phys.*, 38 (1967) 1001.
9. K.H.J. Buschow, W. Luiten. P.A. Nastepadet, *Philips. Tech. Rew.*, 29 (1968) 336.
10. J.J. Croat, J.F. Herbst, R.W. Lee, F.E. Pinkerton, *Appl. Phys. Lett.*, 44 (1984) 148.
11. S.K. Andwer, *J. Appl. Phys.*, 81 (1997) 5609.
12. H.A. Luepold, E. Potenziani, J.P. Clkare, A. Tauber, *IEEE Trans. Magn.*, 20 (1984) 1572.
13. S. Liu, E. Kuhl, *IEEE Trans. Magn.*, 35 (1999) 3271.
14. G. Goll, H. Stadelmaier, H. Kronmüller, *Scripta Mater.*, 63 (2012) 243.
15. H. Kronmüller, G. Goll, *Scripta Mater.*, 48 (2003) 833.
16. M. Rajasekhar, D. Akhtar, V. Chandrasekaran, S. Ram, *J. Alloys Compd.*, 480 (2009) 670.
17. S.G. Kim, M.J. Kim, K.S. Ryu, Y.B. Kim, C.S. Kim, T.K. Kim, *IEEE Trans. Magn.*, 35 (1999) 3316.
18. Z.A. Chen, J. Luo, Y.L. Sui, Z.M. Guo, *J. Rare Earth*, 28 (2010) 277.
19. C.H. Chiu, H.W. Chang, C.W. Chang, W.Y. Zhang, W.C. Chang, *J. Iron Steel Res. Int.*, 13 (2006) 136.
20. H.W. Chang, J.Y. Gan, C.C. Hsieh, X.G. Zhao, W.C. Chang, *J. Appl. Phys.*, 107 (2010) 09A740.
21. M.X. Pan, P.Y. Zhang, H.L. Ge, Q. Wu, *Mater. Technol.*, 31 (2016) 580.
22. A. Gebert, A.A. El-Moneim, O. Gutfleisch, L. Schultz, *IEEE Trans. Magn.*, 38 (2002) 2979
23. X.G. Cui, M. Yan, T.Y. Ma, L.Q. Yu, *Physica B*, 403 (2008) 4182
24. J.T. Li, M.X. Pan, Y.D. Yu, H.L. Ge, Q. Wu, *Int. J. Electrochem. Sci.*, 13 (2018) 8897.
25. Y. Zhang, G.C. Hadjipanayis, *IEEE Trans. Magn.*, 40 (2004) 2925.

© 2020 The Authors. Published by ESG ([www.electrochemsci.org](http://www.electrochemsci.org)). This article is an open access article distributed under the terms and conditions of the Creative Commons Attribution license (<http://creativecommons.org/licenses/by/4.0/>).